Green and chemically synthesized magnetic iron oxide nanoparticles-based chitosan composites: preparation, characterization, and future perspectives

Mohamed S. Elnouby[1,*] (iD), Tarek H. Taha[2], M. A. Abu-Saied[3], Saad A. Alamri[4,5], Yasser S. M. Mostafa[4], and Mohamed Hashem[4,6]

[1] *Composite and Nanostructured Materials Research Department, Advanced Technology and New Materials Research Institute, City of Scientific Research and Technological Applications (SRTA-City), New Borg El-Arab City 21934, Alexandria, Egypt*

[2] *Environmental Biotechnology Department, Genetic Engineering and Biotechnology Research Institute (GEBRI), City of Scientific Research and Technological Applications (SRTA-City), New Borg El-Arab City 21934, Alexandria, Egypt*

[3] *Polymer Materials Research Department, Advanced Technology and New Materials Research Institute, City of Scientific Research and Technological Applications (SRTA-City), New Borg El-Arab City 21934, Alexandria, Egypt*

[4] *Department of Biology, College of Science, King Khalid University, Abha 61413, Saudi Arabia*

[5] *Prince Sultan Ben Abdulaziz Center for Environmental and Tourism Research and Studies, King Khalid University, Abha, Saudi Arabia*

[6] *Faculty of Science, Department of Botany and Microbiology, Assiut University, Assiut 71516, Egypt*

ABSTRACT

Magnetic nanoparticles have recently attained much interest due to the wide distribution of their applications. The current work is concerned with the synthesis of magnetic iron oxide nanoparticles using green and chemical methods. Licorice extract has been used as the main factor for the production of green synthesized magnetic nanoparticles (GSM), compared with the co-precipitation method for the production of chemically synthesized magnetic nanoparticles (CSM). Both scanning electron microscopy (SEM) and particle size analyzer (PSA) proved the formation of the particles in the nanoscale with the range of 50–110 nm and 40–100 nm for GSM and CSM, respectively. Furthermore, Energy-dispersive X-ray spectroscopy (EDX) indicated the existence of iron and oxygen elements in both the samples and proved the formation of iron oxide nanoparticles. Both types of nanoparticles were solely integrated with chitosan for the formation of magnetic-dependent membranes followed by integration-dependent characterization using SEM and Raman spectroscopy. The tensile properties of the membranes showed higher elongation and strain properties of chitosan/GSM membrane compared with plain chitosan or chitosan/CSM membranes, which candidate it for mechanical-dependent applications. The vibrating sample magnetism (VSM) properties showed that GSM nanoparticles are superparamagnetic. In addition, the GSM nanoparticles are applied as

Address correspondence to E-mail: m_nano2050@yahoo.com

Springer

methanol electrochemical sensors with high sensitivity even at low concentrations of methanol.

1 Introduction

Metal nanoparticles have a higher Fermi potential, which leads to the lowering of their reduction potential and makes them useful in catalyzing the reactions responsible for electron transfer [1]. Iron oxide has attracted a considerable academic and technological interest for a variety of applications, such as water treatment, drug delivery [1], catalysis, water splitting, imaging, chemical energy conversion and storage technologies [2], sensors/bio-sensors [3, 4], and biomedical applications [5].

Iron oxide nanoparticles have been successfully fabricated by a variety of methods, including wet-dependent chemical methods [3, 5], liquid phase deposition [2], and the eco-friendly preparation method. The green synthesis of nanoparticles using biological materials such as plants and plant extracts has been proposed as a cost-effective and environmentally friendly method that could be used as an alternative for chemical and physical methods. It has the advantage of being formed at an ambient temperature and neutral pH. In addition, it is a low-cost method, requires low maintenance, and does not release toxic materials to the environment [6]. Polymeric substances are particularly attractive due to the presence of a variety of surface functional groups, excellent mechanical properties, and a large area of production. Among all, chitosan—a poly-cationic biopolymer derived from chitin—is a promising polymer and the second most usable biopolymer in nature [7]. On the other hand, magnetic particles tend to aggregate by nature, which could be prevented if they were surrounded by a polymeric substance [8]. Among all natural polymers that have been examined, chitosan is often chosen as a supporting material for preparing magnetic materials due to its superior biodegradability, biocompatibility, low cytotoxicity, unique chemical properties, and large economic production ability [9–11]. A magnetic chitosan composite (MCC) consists of a chitosan matrix mixed with distributed magnetic particles. Magnetic chitosan materials are helpful in various fields for biomedical applications such as anti-cancer embolotherapy, targeting drug carriers, bone

regeneration, artificial muscles, enzyme-based bio-fuel cells [12–14], and environmental (pollutant removal and toxic pollutant degradation) [15] and analytical (biosensor, separation, affinity chromatography, fluorescence probes) applications [16]. Magnetic nanoparticles are known for their higher chemical activity and easiest oxidation in air, which results in a loss of magnetism and dispersibility [17]. Coating of magnetic particles with chitosan will show multiple advantages of protection from oxidation, reduction of toxicity, reduction of aggregation, and an extended storage life [18]. Interestingly, a chitosan coating not only stabilizes the magnetic particles but it can also be used as a surface for further functionalization (due to the existence of various functional groups, such as carboxyl groups, abundant amino groups, and hydroxyl groups) with specific components such as catalytically active species, specific binding sites, various drugs, or other chelating functional groups which will improve the adsorption performance of magnetic chitosan [19]. Furthermore, chitosan has a considerable ability to form metal chelates and pH responsiveness, which are useful in the preparation of MCCs and can be easily modified by chemical or physical procedures to prepare chitosan derivatives that contain new functional groups. Well-articulated reviews are available to understand the physicochemical characterization of chitosan [20]. The aim of the current study was to compare green synthesized and chemically synthesized magnetic nanoparticles and find out which one is suitable for application when used individually or when integrated with an interesting polymeric material such as chitosan. The target achievement depended on the characterization of nanoparticles before and after integration into chitosan, followed by the experimental investigation of their degree of magnetism and electrochemical properties.

2 Experimental

2.1 Materials

All chemicals used here were of analytical grade and were used without any further purification. Iron (III) chloride hexahydrate (FeCl$_3$.6H$_2$O) (98%) and Iron (II) chloride tetrahydrate (FeCl$_2$.4H$_2$O) (98%) were purchased from Sigma-Aldrich as the iron precursor, while the precipitating agent ammonium hydroxide (NH$_4$OH) solution (30 ∼ 33%) was purchased from Sigma-Aldrich. Chitosan (purity > 90%) was purchased from Biobasic, Canada, while Acetic acid (assay ≥ 99%) was obtained from Sigma-Aldrich Chemicals, Ltd.(Germany). The powder form of licorice was purchased from a local herbaceous market in New Borg El-Arab city, Alexandria, Egypt.

2.2 Preparation of plant extract

Hot water extract of licorice roots (*Glycyrrhiza glabra* L) was prepared by boiling 100 ml distilled water containing 10 g of licorice powder for 10 min. After the extract cooled down, the mixture was centrifuged at 10.000 rpm for 15 min. After centrifugation, the supernatant was filtrated using Whatman filter paper No 1 (11 μm particle size range) to remove any floated plant debris that was used for green synthesis of magnetite nanoparticles.

2.3 Synthesis of magnetic nanoparticles

2.3.1 Green synthesis

The biosynthesis of Fe$_2$O$_3$ nanoparticles (magnetite nanoparticles) was achieved using equal volumes of 1 M FeCl$_3$ and licorice extract. The whole process depended on the drop-wise flow of the metal solution into a 150 rpm stirred solution of the plant extract at room temperature. The formed black particles were collected by centrifugation at 10.000 rpm for 20 min, followed by washing twice with absolute ethanol and once with distilled water. The washed magnetic nanoparticles were kept at 40 °C for 18 h till full dryness.

2.3.2 Chemical synthesis

The magnetite nanoparticles were prepared by a co-precipitation method as described by [5]. Briefly,

16.25 g of FeCl$_3$·6H$_2$O and 6.5 g of FeCl$_2$·6H$_2$O were dissolved in 150 ml of deionized water under magnetic stirring for 30 min at 80 °C. The solution was bubbled with nitrogen gas to prevent undesirable oxidation. Then, ammonium hydroxide (50 ml, 25%) was added to the iron solution. After 1 h, the resulting magnetic nanoparticles were gathered from the solution by magnetic separation, washed several times with deionized water and once with ethanol, and then dried under vacuum conditions at 60 °C for 12 h.

2.4 Characterization of GSM and CSM

The morphological structures of the GSM and CSM nanoparticles were performed using scanning electron microscopy (SEM, JEOL, JSM-6360LA, Japan) and transmittance electron microscopy (TEM, JEOL, JEM2100 plus, Japan). The main particle sizes were measured by the particle size analyzer (PSA, Beckman Coulter, USA). The elemental analysis of samples was detected using Energy-dispersive X-ray spectroscopy (EDX) at acceleration volt of 15 kV. The crystalline structures were examined using X-ray diffraction (XRD, Shimadzu, 400, Japan), and the crystal size has been calculated using the Debye Scherer equation [21]:

$$D = 0.9\lambda/\beta \cos\theta.$$

where λ is the X-ray wavelength, β is the line broadening at half the maximum intensity in radians, and θ is the Bragg angle. The magnetic properties of GSM and CSM nanoparticles were investigated at room temperature using a vibrating sample magnetometer (VSM, 7410-S, Lake Shore Cryotronics Inc., USA).

2.5 Preparation of chitosan/GSM and chitosan/CSM membranes

A total volume of 20 ml of chitosan solution (2%) was dissolved in 1% acetic acid. Both GSM and CSM were separately added to the chitosan solution (Solution A and B, respectively), with overnight continuous stirring at 30 °C. The final reactant solutions were separately cast in Petri dishes and kept at room temperature for two days till full dryness. A magnetic nanoparticles-free chitosan solution (as a control) was also prepared and cast in a Petri dish and subjected to the same polymerization conditions.
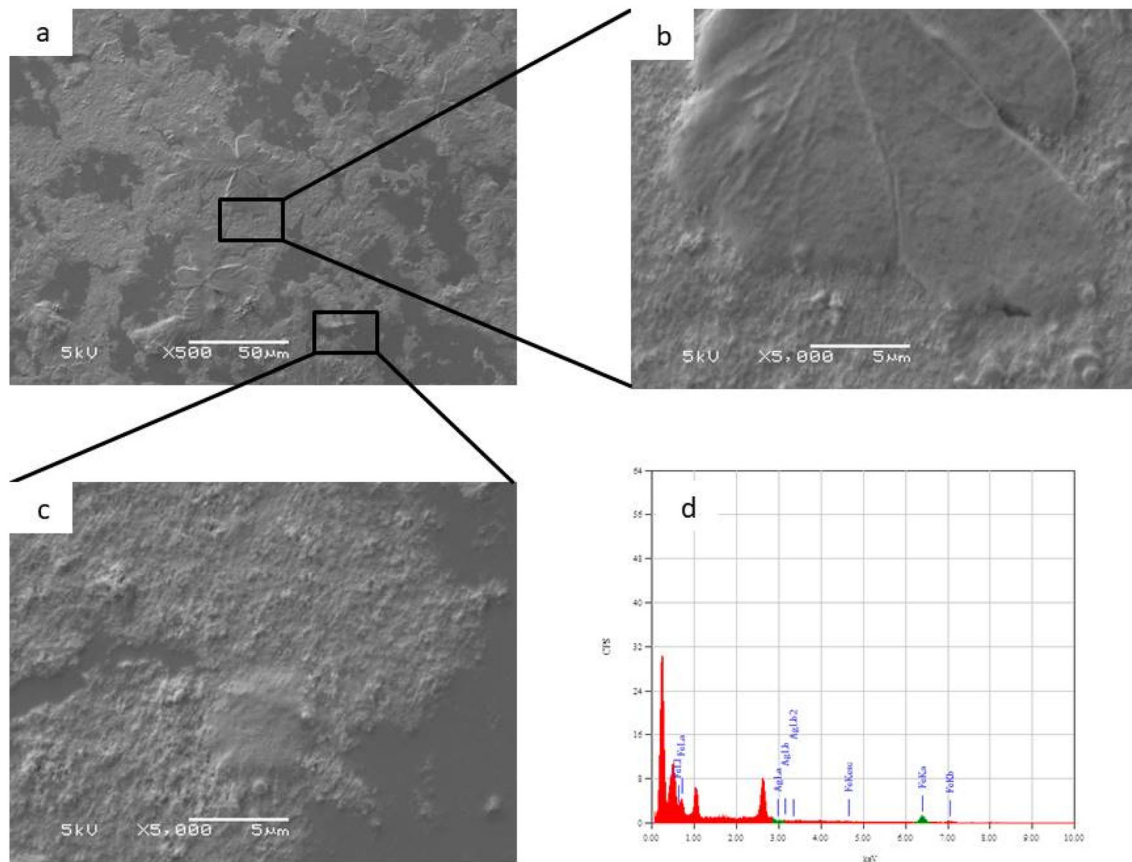
Fig. 1 Scanning electron micrographs of GSM (**a**, **b**, and **c** are the obtained micrographs at various locations and magnifications); while **d** is the EDX analysis of GSM
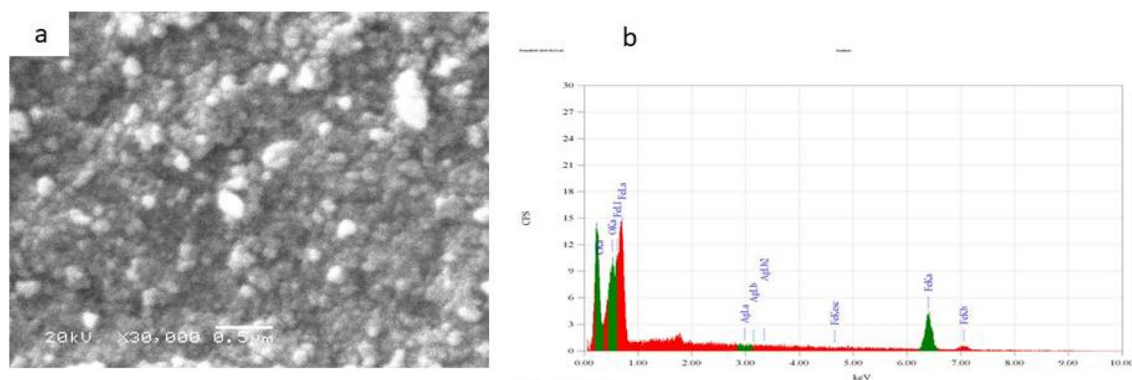

Fig. 2 Scanning electron micrographs of CSM (**a**); while **b** is the EDX analysis of CSM

2.6 Characterization of membranes

A Raman scattering spectrometer (SENTERRA-Bruker, Germany) was used to investigate the chemical structure of the prepared polymeric membrane. The tensile strength of the polymeric membranes was measured using the Universal Testing Machine (Shimadzu UTM, Japan) [22]. The morphological features of the membranes were also examined using scanning electron microscopy (SEM, JEOL JSM-6360LA, Japan). Electrochemical cyclic voltammetry was carried out using a computer-controlled potentiostat (Metrohm Autolab, model: 87,070). All the obtained instrumental characterizations were performed for
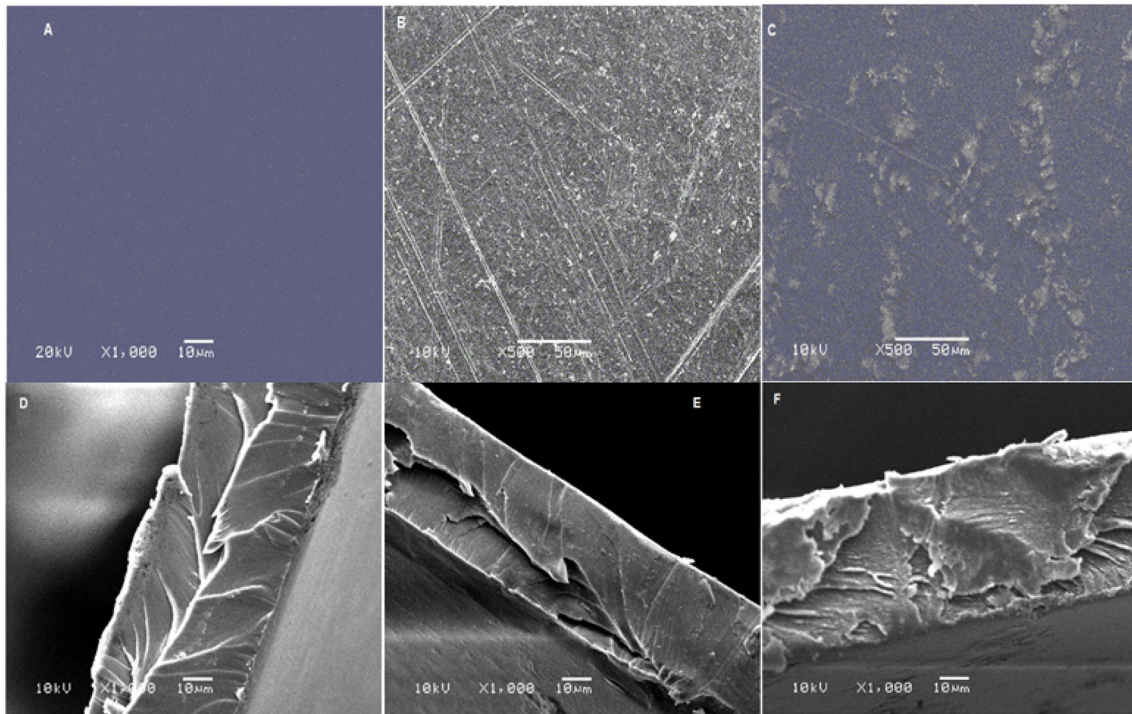
Fig. 3 Morphological appearance of the surfaces and cross-sections of chitosan, chitosan/GSM, and chitosan/CSM membranes. **A**: the surface of chitosan membrane, **B**: the surface of chitosan/CSM membrane, **C**: the surface of chitosan/GSM membrane, **D**: the cross-section of chitosan membrane, **E**: the cross-section of chitosan/CSM membrane, and **F**: the cross-section of chitosan/GSM membrane

plain chitosan, chitosan/GSM, and chitosan/CSM membranes.

2.7 Kinetic models

The investigations of the mechanism of sensing took place using two kinetic models: the pseudo-first-order model and pseudo-second-order model. The pseudo-first-order equation is represented as follows [23]:

$$\ln(M_e - M_d) = \ln M_e - K_1 D$$

where M_e and M_d are the sensing current (A) at equilibrium and at concentration (D), respectively, and k_1 is the sensing rate.

The pseudo-second-order model can be expressed by the following equation [23]:

$$\frac{d}{M_d} = \frac{1}{K_2 M_e^2} + \left(\frac{1}{M_d}\right) D$$

where K_2 is the sensing rate. M_e and K_2 can be determined from the slope and intercept of the plot.

The initial sensing rate (h) could be calculated from pseudo-second-order by using the following formula [23]:

$$h = K M_e^2.$$

3 Results and discussion

3.1 Characterization

3.1.1 Morphological structure

3.1.1.1 SEM Figure 1 displays the scanning electron micrographs of GSM where the obtained nanoparticles were uniform and spherical. The obtained nanoparticles' size is in the range of 50–110 nm. These nanoparticles have been detected to be associated with outer leaf-like shapes, which could be attributed to the physical adsorption of biomaterials of the used plant extract (Fig. 1b). Previous studies proved the physical bond of produced biomaterials such as proteins to the surface of produced nanoparticles [24–27]. The chemically synthesized iron oxide nanoparticles were presented in Fig. 2a. It

Fig. 4 TEM micrographs of **a** GSM and **b** CSM nanoparticles
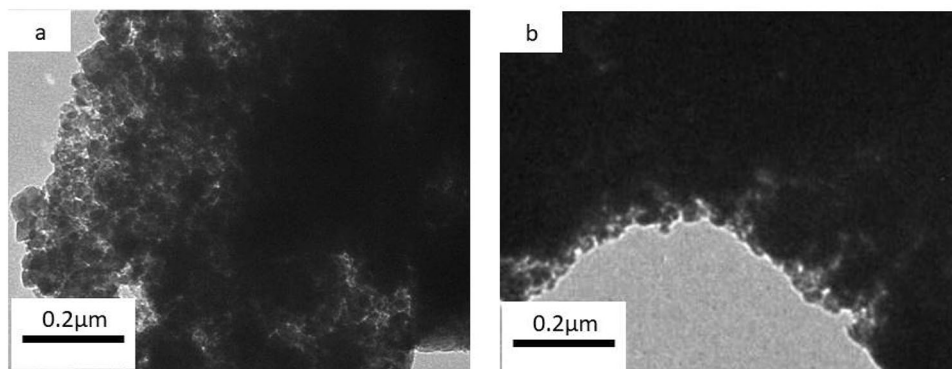
is noticeable that the obtained nanoparticles were in a spherical shape with sizes ranging from 40–100 nm. While scanning electron micrographs of the surface of chitosan, chitosan/GSM and chitosan/CSM membranes are shown in Fig. 3A, B, and C. The difference in the morphology between the surfaces of chitosan, chitosan/GSM, and chitosan/CSM is quite obvious. Chitosan (Fig. 3A) appears to have a smooth and homogeneous surface, which is probably caused

by the presence of extensive hydrogen bonding between the functional groups of the polymer (–OH and –NH$_2$ groups in chitosan) [28]. However, the formation of Fe$_2$O$_3$ nanoparticles on the surfaces of chitosan/GSM and chitosan/CSM is almost associated with the display of rough and heterogeneous appearances (Fig. 3A and C). There was no significant change in the three micrographs of the cross-sections of the membranes. The chitosan cross-section approximately has the same appearance as chitosan/GSM and chitosan/CSM cross-sections, which indicates the exclusive distribution of the nanoparticles on the surfaces of the two membranes with absolute absence internally (Fig. 3D, E and F).

3.1.1.2 TEM Figure 4 presents the transmittance electron micrographs of the green and chemically synthesized iron oxide nanoparticles. As shown in Fig. 4a (GSM), the formed nanoparticles are in a
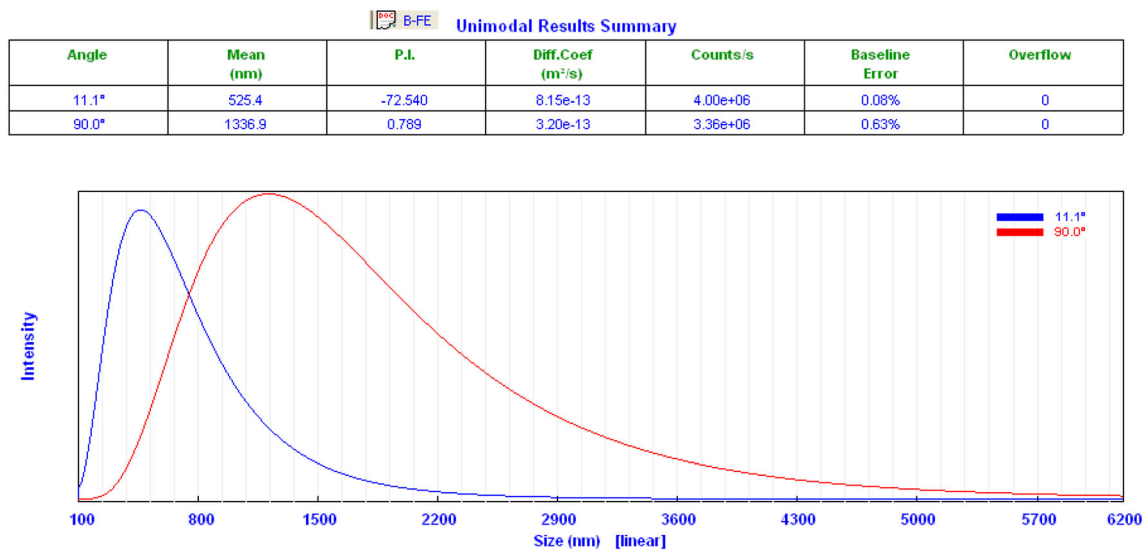
Table 1 EDX analysis of GSM and CSM samples

Elements	CSM			GSM		
	KeV	Mass %	K	KeV	Mass %	K
Fe	6.39	63.89	76.72	6.39	92	93
O	0.525	10.16	12.4	0.525	6.8	7
Other (H)	0.277	25	10	–	–	–

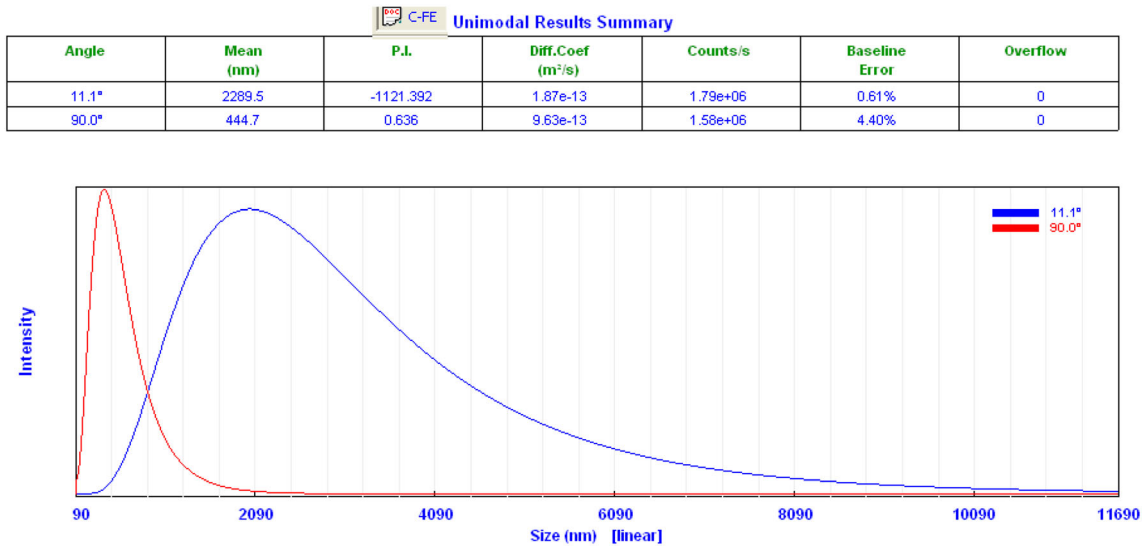**Fig. 5** Particle size distribution histogram of GSM

Fig. 6 Particle size distribution histogram of CSM

polygon shape with a size distribution from 15 to 70 nm. However, the CSM nanoparticles showed more aggregation with less size distribution from 15 to 50 nm (Fig. 4b). These results are matched with the size distribution that has been measured from SEM micrographs.
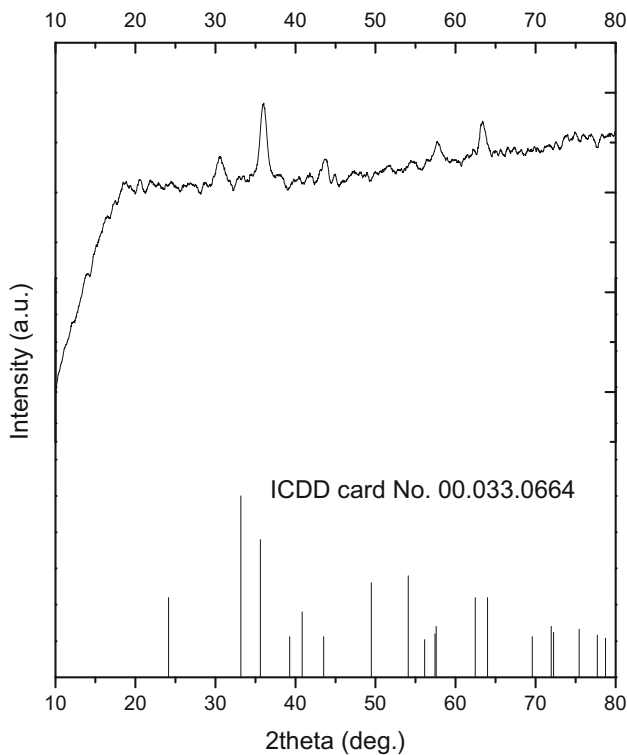

Fig. 7 XRD pattern of the CSM sample

3.1.2 Energy-dispersive X-ray spectroscopy (EDX)

Energy-dispersive X-ray spectroscopy (EDX) is an analytical technique used for elemental analysis. It reflects the percentage and kind of each element that has already existed in the tested sample. Figures 1d and 2b show the EDX of GSM and CSM samples with the current investigation of the percentage and type of each element. The peak around 0 6.4 keV is related to the binding energies of the Fe element, along with the peak of oxygen at 0.5 keV. Therefore, the EDX confirmed the presence of both iron and oxygen in the tested nanoparticles. Table 1 summarizes the EDX results for both the green synthesized and chemically synthesized iron oxide nanoparticles. The EDX analysis confirms the formation of iron oxide nanoparticles. The iron/oxygen ratio was 93/7 for GSM and 76.7/12.4 for CSM. Our results are matched but are better than the data obtained by Jagathesan and Rajiv who prepared iron oxide nanoparticles via the green method. Their obtained nanoparticles showed 77.08%

Table 2 The size distribution of GSM and CSM nanoparticles

Size distribution (nm)			
	SEM	TEM	XRD
GSM	50–110	15–70	–
CSM	40–100	15–50	9

Table 3 Tensile strength, elongation, stress, and strain of chitosan, chitosan/GSM, and chitosan/CSM membranes

Sample	T.S (N)	Elongation (mm)	Max Stress (N/mm^2)	Max Strain (%)
Chitosan	26.0938	1.16400	37.2768	3.88000
Chitosan/GSM	21.2500	7.07450	30.3571	23.5817
Chitosan/CSM	9.21875	0.35700	15.3646	1.19000

Fig. 8 Raman spectrum of chitosan, chitosan/GSM, and chitosan/CSM
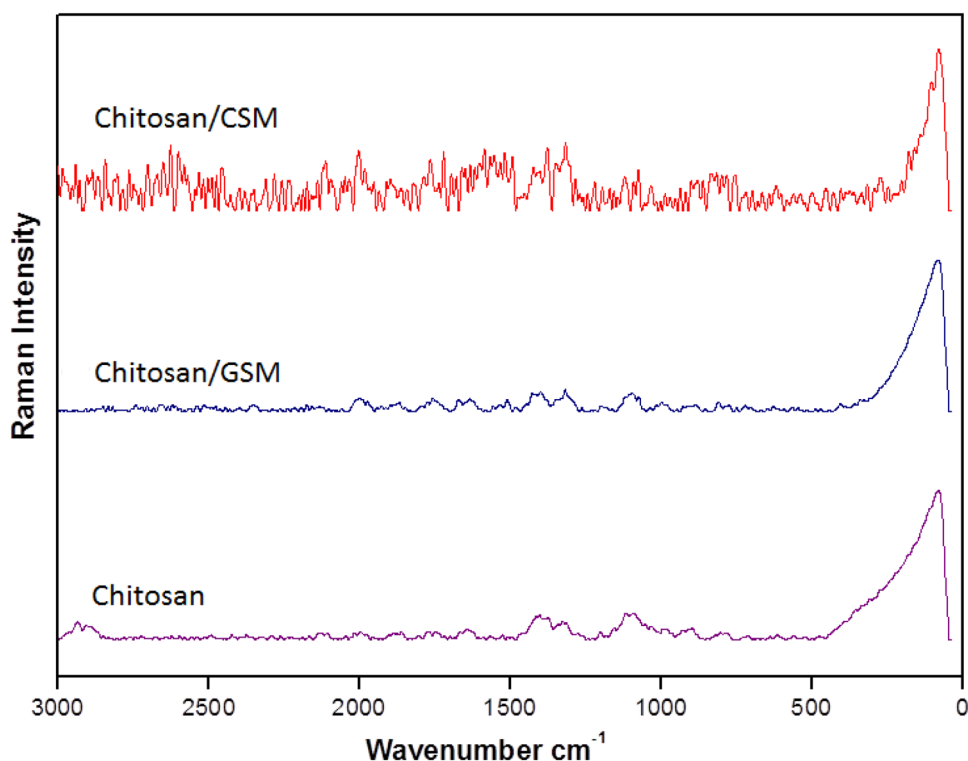
of iron and 22.97% of oxygen, as reported by the EDX analysis [29].

3.1.3 Particle size analysis

Figure 5 shows the particle size distribution histogram of green synthesized iron oxide nanoparticles. As detected by the machine analysis, the main particle size is approximately 525 nm. Figure 6 shows the particle size distribution histogram of chemically synthesized iron oxide nanoparticles, which indicated that the main particle size is almost 444 nm. It could be noticed that the particle size observed by the PSA method is larger than that observed by other techniques such as SEM. This may be attributed to the magnetic properties (magnetic dipole–dipole interaction) of the prepared nanoparticles that result in the particles having a great tendency to bind and be attracted to each other and appear as aggregated

clusters [30]. On the other hand, the observed particle size of GSM is much greater than the particle size of CSM, which might be related to the existence of biomolecules as an outer shell on the GSM, and hence would result in larger aggregated particles.

3.1.4 X-Ray diffraction (XRD)

The XRD pattern is one of the most important characterization techniques for the identification of nanoparticles. As shown in Fig. 7, all the observed peaks can be indexed to the rhombohedral (hexagonal) structure of hematite α-Fe$_2$O$_3$ (space group: R-3c), with lattice constants of a = 0.5034 nm and c = 1.375 nm (ICDD Card No. 00.033.0664). This result is in a good agreement with that obtained by Lassoued and his colleagues, who reported a similar XRD pattern of chemically synthesized iron oxide nanoparticles [31]. According to the data obtained
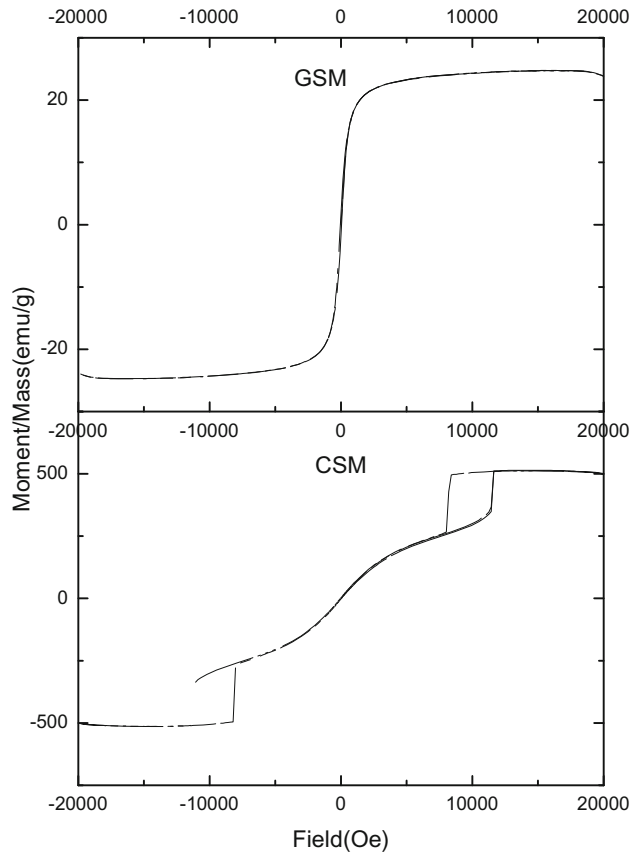
Fig. 9 Magnetic Hysteresis loop of GSM and CSM nanoparticles

Fig. 10 Cyclic voltammogram (CV) of GSM and CSM nanoparticles
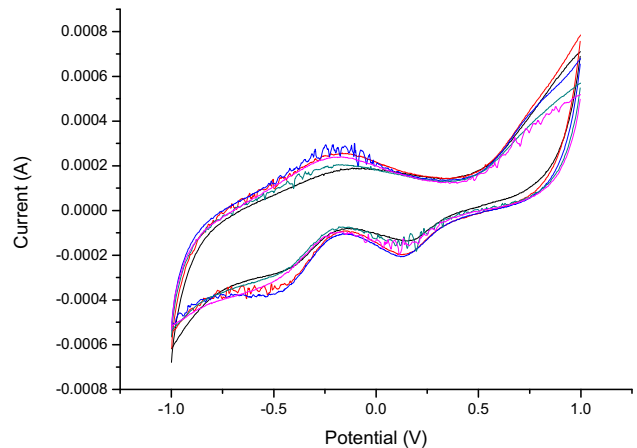
Fig. 11 Cyclic voltammogram of the prepared electrode in buffer solution (pH 7.0) with different amounts of methanol

from the Debye Scherer equation, the crystal size of the CSM sample was calculated as 9 nm. This calculated crystal size is lower than the observed particle size that has been measured from SEM and TEM micrographs. This is attributed to the fact that the Debye Scherer equation only calculates the crystal size without aggregation while the SEM and TEM micrographs measure the size of the particles, not the crystals.

The size distribution of GSM and CSM nanoparticles by SEM, TEM, and XRD are summarized in Table 2.

3.2 Characterization of chitosan/GSM and chitosan/CSM membranes

3.2.1 Tensile strength

The tensile properties of tensile strength, elongation, stress, and strain were measured, and the results are listed in Table 3. With the addition of iron oxide nanoparticles to the chitosan polymer, the tensile strength decreased from 26.0938 N to 21.25 N (for
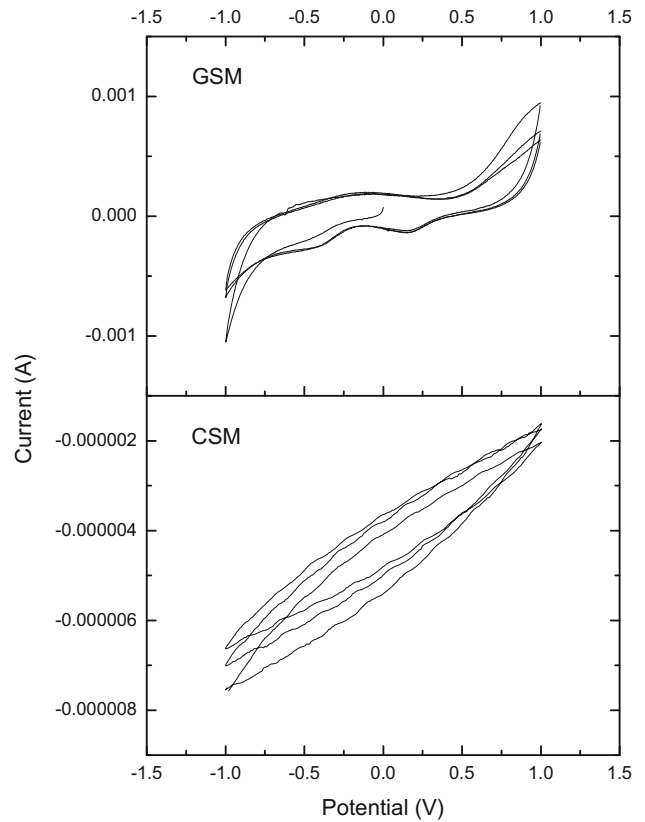
chitosan/GSM) and 9.21875 N (for chitosan/CSM), while the elongation increased from 1.164 mm to 7.0745 mm (for chitosan/GSM), but decreased to 0.357 mm (for chitosan/CSM). The strain increased from 3.88% chitosan to 23.5817% chitosan/GSM, and decreased to 1.19000% for chitosan/CSM. The overall
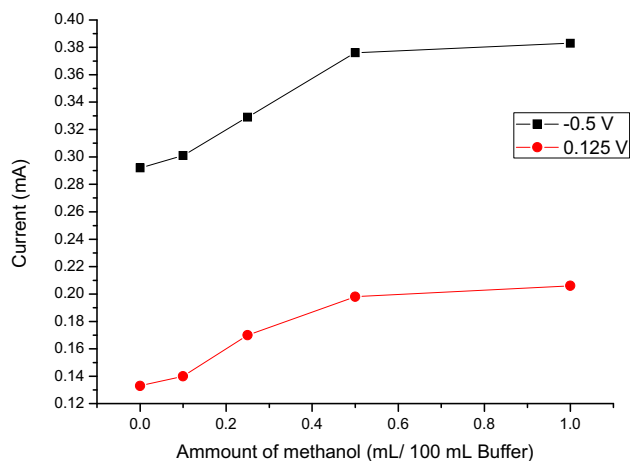
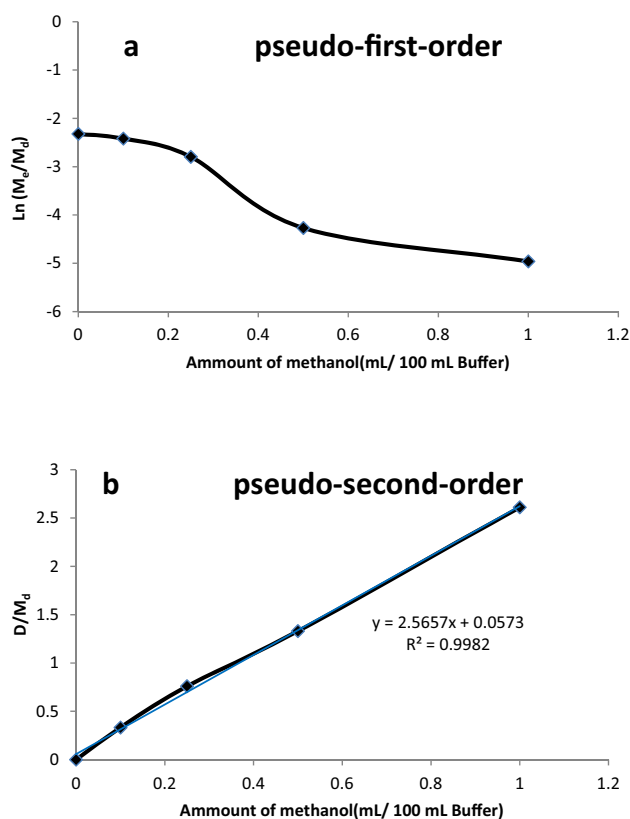**Fig. 12** Calibration curves obtained from methanol at -0.5 V and + 0.125 V

Fig. 13 Kinetics **a** pseudo-first order and **b** pseudo-second order models

Table 4 Kinetics parameters

Parameter	R^2	$M_{e\ (exp)}$	$M_{e\ (calc)}$	K	h
Value	0.9982	0.39	0.389	114.74	0.0087

obtained results revealed the proper selection of chitosan/GSM membranes in applications with improved tensile strength properties.

3.2.2 Raman scattering spectra

The Raman scattering spectrum of the chitosan membrane has been shown in Fig. 8. This spectrum exhibited a strong valence band at 1656 cm^{-1} due to the C = O bond. Also, the chitosan spectrum revealed signals at 1119.30 cm^{-1} and 1433.19 cm^{-1}, which are attributed to vibrations of several C–C and C-H present in the CHS chains, respectively. The Raman scattering spectrum of α-Fe$_2$O$_3$ was taken at room temperature with a 5309 A° laser line. The peak at 1320 cm^{-1} is due to the two magnon scattering samples from different sources (Green and chemical synthesis) that were studied, and both gave similar results.

3.3 Features-depending applications

3.3.1 Vibrating sample magnetism (VSM)

To study the magnetic properties of both GSM and CSM, magnetic hysteresis loops were recorded using VSM under the applied magnetic field of 13,000–15,000 Oe at room temperature (Fig. 9). The magnetic properties proved that the GSM nanoparticles were superparamagnetic with a saturation magnetization (Ms) value of 24.76 emu g^{-1}, while CSM nanoparticles have saturation magnetization (Ms) values of 514.5 emu g^{-1} with some magnetic memory features. The magnetization features of GSM make it the most suitable candidate material for biomedical applications, such as hyperthermia therapy [32]. These magnetic properties results are in a good agreement with the data obtained by Ogholbeyg and his colleagues [33]. Table 5 represents and compares among the other data published in the literature.

3.3.2 Electrochemical behavior

To evaluate the electrochemical catalytic activities of both GSM and CSM, cyclic voltammetry was carried out using a computer-controlled potentiostat (Metrohm Autolab, model: 87,070). The prepared electrodes (chitosan/GSM or chitosan/CSM) were used as working electrodes, platinum (Pt) wire as a

Table 5 Comparison of iron oxide-based magnetic nanoparticles prepared by various methods and their characteristics

Material	Preparation	Size (nm)	Saturation magnetization (Ms) (emu g^{-1})	Application	REF
CSM	Chemical precipitation	9 ∼ 100	514.5		Current study
GSM	Green synthesis	15 ∼ 110	24.76	Sensor	Current study
MNP	Green synthesis	48.9 ∼ 85	0.88 ∼ 23.04	Antimicrobial and antioxidant activity	[35]
Fe2O3/C	Hydro-thermal co-precipitation	5 ∼ 30	30.3	Antioxidant	[36]
Reduced graphene oxide/iron oxide (RGO/Fe$_3$O$_4$)	Green synthesis	–	12.6 ∼ 15.3	Heavy metal removal	[37]
Superparamagnetic maghemite	Green synthesis	7 ∼ 12	53	Bio application	[33]

counter electrode, and saturated calomel electrode (SCE) as a reference electrode using phosphate buffer solution (PBS) (pH 7.0) as the electrolyte. Figure 10 shows the cyclic voltammograms of the prepared membranes between -1 V and + 1 V. The chitosan/CSM electrode showed a peakless oxidation/reduction behavior (Fig. 10). Otherwise, the chitosan/GSM electrode showed a significant peak in the reduction scan higher than those of the chitosan/CSM electrode (Fig. 10), which suggests it is a biosensor electrode [34].

3.3.2.1 Biosensing application Figure 11 shows the cyclic voltammogram of the prepared chitosan/GSM electrode between -1 V and + 1 V. The biosensor response was tested in a 100 ml buffer solution (pH 7.0) with the presence of a different amount of methanol (0.001 ∼ 0.01 volume ratios). It is noticeable that there are two response ranges at (+ 0.125 V) and (-0.53 V). The calibration curves of these two ranges are presented in Fig. 12. The obtained material, which was started with very low concentrations of methanol, has remarkable electrochemical resonance to methanol.

3.3.2.2 Modeling of sensing kinetics To model the kinetics of the sensing interaction, both the pseudo-first order and pseudo-second order models have been used to fit the experimental sensing curves shown in Fig. 11. Figure 13 shows the pseudo-first order and pseudo-second order models of the calibration sensing curve at -0.5 V. It is noticeable that the pseudo-first order model is non-linear (Fig. 13-a),

whereas the pseudo-second order model shows linear behavior (R^2 = 0.9982) (Fig. 13-b). According to the linearity behavior of the pseudo-second order model, the further calculations of kinetic parameters will be performed depending on the pseudo-second order model equation. Table 4 summarizes these kinetics parameters.

3.3.2.3 Biosensing mechanism According to the previous measurements, the sensing mechanism could be described as follows: first, methanol was adsorbed on the surface of GSM nanoparticles, followed by the electrochemical reaction that occurred through the electro-degradation steps. The resulting intermediate organic species were interacted on the electrode surface [31]. Finally, the adsorbed species affected the electrochemical behavior of the electrode. These superior features of GSM are due to the preparation conditions. The green synthesis method depends on enzymatic extract, where in situ self-assembly process takes place [32]. The obtained well-oriented small nanoparticles did not form domain walls and showed superparamagnetic properties [33]. Table 5 provides a comparison of iron oxide-based magnetic nanoparticles prepared by various methods and their characteristics.

4 Conclusion

Two types of iron oxide magnetic nanoparticles—green synthesized magnetic nanoparticles (GSM), and chemically synthesized magnetic nanoparticles

(CSM)—have been prepared. All the prepared materials were on the nanoscale as proved by the characterization techniques of SEM and PSA. Chitosan-based membranes have been prepared by mixing the magnetic nanoparticles with chitosan. The evaluated magnetic nanoparticles and membranes showed superior features. GSM nanoparticles have been recommended as a candidate material for biomedical applications, while CSM nanoparticles have been recommended as a promising material for chemical energy conversion and storage applications.

Acknowledgement

References

1. J.-R. Chiou, B.-H. Lai, K.-C. Hsu, D.-H. Chen, One-pot green synthesis of silver/iron oxide composite nanoparticles for 4-nitrophenol reduction. J. Hazard. Mater. **248**, 394–400 (2013)

2. S.N. Khatavkar, S.D. Sartale, α-Fe2O3 thin film on stainless steel mesh: A flexible electrode for supercapacitor. Mater. Chem. Phys. **225**, 284–291 (2019)

3. P. Das, B. Mondal, K. Mukherjee, Facile synthesis of pseudo-peanut shaped hematite iron oxide nano-particles and their promising ethanol and formaldehyde sensing characteristics. RSC Adv. **4**, 31879–31886 (2014)

4. I. Koh, L. Josephson, Magnetic nanoparticle sensors. Sensors **9**, 8130–8145 (2009)

5. M. Mahdavi, M. Ahmad, M. Haron, F. Namvar, B. Nadi, M. Rahman, J. Amin, Synthesis, surface modification and characterisation of biocompatible magnetic iron oxide nanoparticles for biomedical applications. Molecules **18**, 7533–7548 (2013)

6. K. Parveen, V. Banse, L. Ledwani, Green synthesis of nanoparticles: their advantages and disadvantages, in: AIP conference proceedings, AIP Publishing LLC, 2016, pp. 020048.

7. R.A. Muzzarelli, J. Boudrant, D. Meyer, N. Manno, M. DeMarchis, M.G. Paoletti, Current views on fungal chitin/chitosan, human chitinases, food preservation, glucans, pectins and inulin: A tribute to Henri Braconnot, precursor of the carbohydrate polymers science, on the chitin bicentennial. Carbohyd. Polym. **87**, 995–1012 (2012)

8. G. Dodi, D. Hritcu, G. Lisa, M.I. Popa, Core–shell magnetic chitosan particles functionalized by grafting: synthesis and characterization. Chem. Eng. J. **203**, 130–141 (2012)

9. E.B. Denkbaş, E. Kilicay, C. Birlikseven, E. Öztürk, Magnetic chitosan microspheres: preparation and characterization. React. Funct. Polym. **50**, 225–232 (2002)

10. R.A. Muzzarelli, Chitins and chitosans for the repair of wounded skin, nerve, cartilage and bone. Carbohyd. Polym. **76**, 167–182 (2009)

11. J. Singh, M. Srivastava, J. Dutta, P. Dutta, Preparation and properties of hybrid monodispersed magnetic α-Fe2O3 based chitosan nanocomposite film for industrial and biomedical applications. Int. J. Biol. Macromol. **48**, 170–176 (2011)

12. M. Ashokkumar, K.M. Sumukh, R. Murali, N.T. Narayanan, P.M. Ajayan, P. Thanikaivelan, Collagen–chitosan biocomposites produced using nanocarbons derived from goatskin waste. Carbon **50**, 5574–5582 (2012)

13. E.-Y. Chung, H.-M. Kim, G.-H. Lee, B.-K. Kwak, J.-S. Jung, H.-J. Kuh, J. Lee, Design of deformable chitosan microspheres loaded with superparamagnetic iron oxide nanoparticles for embolotherapy detectable by magnetic resonance imaging. Carbohyd. Polym. **90**, 1725–1731 (2012)

14. J.-B. Qu, H.-H. Shao, G.-L. Jing, F. Huang, PEG-chitosan-coated iron oxide nanoparticles with high saturated magnetization as carriers of 10-hydroxycamptothecin: preparation, characterization and cytotoxicity studies. Colloids Surf., B **102**, 37–44 (2013)

15. H. Yan, L. Yang, Z. Yang, H. Yang, A. Li, R. Cheng, Preparation of chitosan/poly (acrylic acid) magnetic composite microspheres and applications in the removal of copper (II) ions from aqueous solutions. J. Hazard. Mater. **229**, 371–380 (2012)

16. L. Liu, L. Xiao, H. Zhu, X. Shi, Preparation of magnetic and fluorescent bifunctional chitosan nanoparticles for optical determination of copper ion. Microchim. Acta **178**, 413–419 (2012)

17. W. Wu, Q. He, C. Jiang, Magnetic iron oxide nanoparticles: synthesis and surface functionalization strategies. Nanoscale Res. Lett. **3**, 397 (2008)

18. W. Zhang, S. Jia, Q. Wu, S. Wu, J. Ran, Y. Liu, J. Hou, Studies of the magnetic field intensity on the synthesis of chitosan-coated magnetite nanocomposites by co-precipitation method. Mater. Sci. Eng., C **32**, 381–384 (2012)

19. W. Zou, H. Geng, M. Lin, X. Xiong, Facile one-pot preparation of superparamagnetic chitosan sphere and its derived hollow sphere. J. Appl. Polym. Sci. **123**, 3587–3594 (2012)

20. C. Pillai, W. Paul, C.P. Sharma, Chitin and chitosan polymers: Chemistry, solubility and fiber formation. Prog. Polym. Sci. **34**, 641–678 (2009)

21. M. El-Desoky, I. Morad, M. Wasfy, A. Mansour, Synthesis, structural and electrical properties of PVA/TiO 2 nanocomposite films with different TiO 2 phases prepared by sol–gel technique. J. Mater. Sci.: Mater. Electron. **31**, 17574–17584 (2020)

22. J. Chen, M. Asano, Y. Maekawa, M. Yoshida, Suitability of some fluoropolymers used as base films for preparation of polymer electrolyte fuel cell membranes. J. Membr. Sci. **277**, 249–257 (2006)

23. W.A. Braun, B.C. Horn, L. Hoehne, S. Stülp, M.B. Rosa, M. Hilgemann, Poly (methylene blue)-modified electrode for indirect electrochemical sensing of OH radicals and radical scavengers. An. Acad. Bras. Ciênc. **89**, 1381–1389 (2017)

24. C.V. Kumar, G.L. McLendon, Nanoencapsulation of cytochrome c and horseradish peroxidase at the galleries of α-zirconium phosphate. Chem. Mater. **9**, 863–870 (1997)

25. I. Macdonald, W. Smith, Orientation of cytochrome c adsorbed on a citrate-reduced silver colloid surface. Langmuir **12**, 706–713 (1996)

26. A. Kumar, S. Mandal, P. Selvakannan, R. Pasricha, A. Mandale, M. Sastry, Investigation into the interaction between surface-bound alkylamines and gold nanoparticles. Langmuir **19**, 6277–6282 (2003)

27. M. Shah, D. Fawcett, S. Sharma, S. Tripathy, G. Poinern, Green synthesis of metallic nanoparticles via biological entities. Materials **8**, 7278–7308 (2015)

28. M. Abu-Saied, R. Wycisk, M.M. Abbassy, G.A. El-Naim, F. El-Demerdash, M. Youssef, H. Bassuony, P.N. Pintauro, Sulfated chitosan/PVA absorbent membrane for removal of copper and nickel ions from aqueous solutions—fabrication and sorption studies. Carbohyd. Polym. **165**, 149–158 (2017)

29. G. Jagathesan, P. Rajiv, Biosynthesis and characterization of iron oxide nanoparticles using Eichhornia crassipes leaf extract and assessing their antibacterial activity. Biocatal. Agric. Biotechnol. **13**, 90–94 (2018)

30. E. Da'na, A. Taha, E. Afkar, Green synthesis of iron nanoparticles by Acacia nilotica pods extract and its catalytic, adsorption, and antibacterial activities. Appl. Sci. **8**, 1922 (2018)

31. A. Lassoued, B. Dkhil, A. Gadri, S. Ammar, Control of the shape and size of iron oxide (α-Fe2O3) nanoparticles synthesized through the chemical precipitation method. Results in physics **7**, 3007–3015 (2017)

32. E. Cheraghipour, S. Javadpour, A.R. Mehdizadeh, Citrate capped superparamagnetic iron oxide nanoparticles used for hyperthermia therapy. J. Biomed. Sci. Eng. **5**, 715 (2012)

33. A.B. Ogholbeyg, A. Kianvash, A. Hajalilou, E. Abouzari-Lotf, A. Zarebkohan, Cytotoxicity characteristics of green assisted-synthesized superparamagnetic maghemite (γ-Fe 2 O 3) nanoparticles. J. Mater. Sci.: Mater. Electron. **29**, 12135–12143 (2018)

34. L. Liu, M. Wang, C. Wang, In-situ synthesis of graphitic carbon nitride/iron oxide− copper composites and their application in the electrochemical detection of glucose. Electrochim. Acta **265**, 275–283 (2018)

35. J.K. Patra, K.-H. Baek, Green biosynthesis of magnetic iron oxide (Fe3O4) nanoparticles using the aqueous extracts of food processing wastes under photo-catalyzed condition and investigation of their antimicrobial and antioxidant activity. J. Photochem. Photobiol., B **173**, 291–300 (2017)

36. K. Bhattacharya, B. Gogoi, A. Buragohain, P. Deb, Fe2O3/C nanocomposites having distinctive antioxidant activity and hemolysis prevention efficiency. Mater. Sci. Eng., C **42**, 595–600 (2014)

37. C. Prasad, P.K. Murthy, R.H. Krishna, R.S. Rao, V. Suneetha, P. Venkateswarlu, Bio-inspired green synthesis of RGO/Fe3O4 magnetic nanoparticles using Murrayakoenigii leaves extract and its application for removal of Pb (II) from aqueous solution. J. Environ. Chem. Eng. **5**, 4374–4380 (2017)

Publisher's Note Springer Nature remains neutral with regard to jurisdictional claims in published maps and institutional affiliations.